AGU PUBLICATIONS

JGR

Journal of Geophysical Research: Space Physics

RESEARCH ARTICLE

10.1002/2017JA024759

Key Points:
- A quasi-linear approach is formulated for the electromagnetic electron cyclotron (EMEC) instability in conditions typical for the solar wind
- The core and halo populations involve distinctively in both the linear and quasi-linear stages of the instability
- Premises are provided for an advanced methodology to characterize, realistically, the EMEC instability and its implication in the solar wind

Correspondence to:
M. Lazar,
marianlazar@yahoo.com

Citation:
Lazar, M., Yoon, P. H., López, R. A., & Moya, P. S. (2018). Electromagnetic electron cyclotron instability in the solar wind. *Journal of Geophysical Research: Space Physics*, *123*, 6–19. https://doi.org/10.1002/2017JA024759

Received 9 SEP 2017
Accepted 3 DEC 2017
Accepted article online 11 DEC 2017
Published online 11 JAN 2018

©2017. American Geophysical Union. All Rights Reserved.

Electromagnetic Electron Cyclotron Instability in the Solar Wind

M. Lazar[1,2], P. H. Yoon[3,4,5], R. A. López[3], and P. S. Moya[6]

[1]Institut für Theoretische Physik, Lehrstuhl IV: Weltraum- und Astrophysik, Ruhr-Universität Bochum, Bochum, Germany, [2]Center for Mathematical Plasma Astrophysics, KU Leuven, Leuven, Belgium, [3]Institute for Physical Science and Technology, University of Maryland, College Park, MD, USA, [4]Korea Astronomy and Space Science Institute, Daejeon, South Korea, [5]School of Space Research, Kyung Hee University, Yongin-Si, South Korea, [6]Departamento de Física, Facultad de Ciencias, Universidad de Chile, Santiago, Chile

Abstract The abundant reports on the existence of electromagnetic high-frequency fluctuations in space plasmas have increased the expectations that theoretical modeling may help understand their origins and implications (e.g., kinetic instabilities and dissipation). This paper presents an extended quasi-linear approach of the electromagnetic electron cyclotron instability in conditions typical for the solar wind, where the anisotropic electrons ($T_\perp > T_\parallel$) exhibit a dual distribution combining a bi-Maxwellian core and bi-Kappa halo. Involving both the core and halo populations, the instability is triggered by the cumulative effects of these components, mainly depending of their anisotropies. The instability is not very sensitive to the shape of halo distribution function conditioned in this case by the power index κ. This result seems to be a direct consequence of the low density of electron halo, which is assumed more dilute than the core component in conformity with the observations in the ecliptic. Quasi-linear time evolutions predicted by the theory are confirmed by the particle-in-cell simulations, which also suggest possible explanations for the inherent differences determined by theoretical constraints. These results provide premises for an advanced methodology to characterize, realistically, the electromagnetic electron cyclotron instability and its implication in the solar wind.

1. Introduction

The in situ measurements in space plasmas reveal local states out of thermal equilibrium (e.g., temperature anisotropies and suprathermal populations) and correlated with enhanced fluctuations, suggesting an important activity of the kinetic instabilities (Alexandrova et al., 2013; Bale et al., 2009; Gary et al., 2016; Hellinger et al., 2006; He et al., 2015; Howes, 2017; Kasper et al., 2003; Stverak et al., 2008; Wilson et al., 2013; Zimbardo et al., 2010). Function of the time and space scales of interest, the evolution of magnetoplasma parcels in the solar wind is frequently associated with weakly unstable perturbations of magnetic field (δB), which grow from some initial level and saturates quasi-linearly at small intensities comparing to the stationary magnetic field ($\delta B^2/B_0^2 < 1$) (Alexandrova et al., 2013; Zimbardo et al., 2010). This quasi-linear turbulence or superposition of waves may coexist with the background (zero order) turbulence resulting from a nonlinear decay of the large-scale perturbations (transported by the supersonic solar wind). The wave fluctuations can be identified as the main source of particle energization (Gaelzer et al., 2008; Pagel et al., 2007; Pavan et al., 2013; Vocks & Mann, 2003; Vocks et al., 2005; Yoon et al., 2016) to explain their non-Maxwellian velocity distributions, which are well fitted by the Kappa power laws (Lazar et al., 2012; Pierrard & Lazar, 2010).

Velocity distributions with a dual structure combining a thermal (Maxwellian) core and a suprathermal halo which enhances the high energy tails of the distribution have been reported by the observations for all species of charged particles, for example, solar wind electrons (Lin, 1998; Maksimovic et al., 2000, 2005; McComas et al., 1992; Pilipp et al., 1987; Stverak et al., 2008), protons in terrestrial magnetosphere (Christon et al., 1988, 1991), and even heavier ions in the solar wind (Collier et al., 1996). During fast winds additional beams are observed enhancing the high-energy populations and generating drifting non-Maxwellian halos and double-humped distributions (Marsch et al., 1982; Pilipp et al., 1987). The halo (subscript *h*) is less dense but hotter than the core (subscript *c*), such that the kinetic energy densities of these two populations are likely to be comparable,

that is, $n_c k_B T_c \sim n_h k_B T_h$. These expectations appear to be confirmed by the Ulysses electron data (Lazar et al., 2015) very often showing events with $\beta_h \sim \beta_c$, where $\beta = 8\pi n k_B T / B_0^2$ is the plasma beta parameter.

A quasi-linear (weakly nonlinear) approach overcomes the limitations of a linear theory and can describe self-consistently the unstable modes developing in nonequilibrium plasmas as well as their back reaction on particle distributions. While having to rely on simulations as a first test of validity (Cuperman, 1981; Davidson & Hammer, 1972; Lazar, Yoon, & Eliasson, 2017; Vocks & Mann, 2003), quasi-linear formalisms are expected to explain the instability saturation and the relaxation of the anisotropic distributions. Despite these challenges, traditional approaches have rested for many decades on a standard bi-Maxwellian description (Cuperman, 1981; Davidson & Hammer, 1972; Gary & Feldman, 1978; Hamasaki & Krall, 1973; Karimabadi et al., 1992; Kennel & Petschek, 1966; Sagdeev & Shafranov, 1961; Vocks & Mann, 2003; Vocks et al., 2005; Yoon et al., 2012). For thermal (or Maxwellian) populations, the saturation states predicted by the quasi-linear theory can reproduce the lower instability thresholds, as inverse correlations between the temperature anisotropy $A = T_\perp / T_\parallel$ (where $\parallel$ and $\perp$ denote directions to the magnetic field), and parallel plasma beta $\beta_\parallel$ (Seough & Yoon, 2012; Seough et al., 2013; Yoon & Seough, 2012). Usually provided by a linear stability theory, the anisotropy thresholds are also expected to conform with the anisotropy limits measured in the solar wind. For the same thermal (core) populations observed in the solar wind this match is indeed confirmed (Hellinger et al., 2006; Stverak et al., 2008). However, the observations do not agree with the contrast between the competing proton cyclotron and mirror instabilities (both driven by an excess of perpendicular temperature $A > 1$): the low-beta anisotropy limits of the solar wind protons does not conform to the lower cyclotron thresholds predicted by the linear theory but aligns better to the mirror thresholds. This paradox seems to be resolved by a quasi-linear approach (Yoon & Seough, 2012), which clearly shows a dominance of mirror instability for low values of the proton beta parameter. An extended quasi-linear investigation becomes therefore crucial for understanding the saturation of growing fluctuations and their effects on particles, which cannot be described by a linear approximation.

Monocomponent bi-Maxwellian models may adapt to thermal (core) populations, but, as shown above, the solar wind electrons exhibit an additional suprathermal halo which is markedly enhanced with increasing the heliospheric distance and the latitude (Maksimovic et al., 2005; Pierrard et al., 2016). Dual models have been introduced by reproducing both the observed core and halo components with idealized (bi-)Maxwellian distribution functions (Feldman et al., 1975; Maksimovic et al., 1997, 2000), and later, these models have also been invoked in studies of their dispersion and stability properties (Gary et al., 1975, 1994; Sarfraz et al., 2016). A recent quasi-linear analysis of the electromagnetic electron cyclotron (EMEC) instability in a two-component electron plasma, both presumably anisotropic and bi-Maxwellian distributed, shows that the enhanced fluctuations may intermediate a transfer of free energy between these populations (Sarfraz et al., 2016).

Nearly Maxwellian at low energies and decreasing as a power law at higher energies, the Kappa distribution function has been introduced as a global empirical model to reproduce and incorporate both the thermal core and suprathermal tails of the velocity distributions observed in the solar wind and terrestrial magnetosphere (Christon et al., 1991; Maksimovic et al., 1997; Olbert, 1968; Vasyliunas, 1968). More convenient in computations, especially due to the reduced number of parameters involved, a global Kappa has been largely adopted in the kinetic studies of plasma waves and instabilities; see reviews by Hellberg et al. (2005) and Pierrard and Lazar (2010). A quasi-linear approach has been recently reported for the EMEC instability in bi-Kappa distributed plasmas (Lazar, Pierrard, et al., 2017) as a test case for the existing numerical setups in particle-in-cell (PIC) (Lu et al., 2010) and Vlasov simulations (Eliasson & Lazar, 2015).

A realistic characterization of the observed (nonstreaming) distributions should combine two distinct components, namely, a bi-Maxwellian core and a bi-Kappa halo (Lazar, Pierrard, et al., 2017; Maksimovic et al., 2005; Stverak et al., 2008). Both are gyrotropic but have different properties and evolutions with the expansion of the solar wind (Maksimovic et al., 2005; Pierrard et al., 2016), which are usually explained by their interactions with the wave fluctuations (Lazar, Pierrard, et al., 2017; Pagel et al., 2007; Wilson et al., 2013; Yoon et al., 2016). However, in a detailed dispersion and stability analysis differentiating between the core and halo populations the computations become cumbersome and only linear approaches of cyclotron instabilities have been reported so far (Lazar et al., 2014, 2015; Shaaban et al., 2017). The unstable regimes are expected to be triggered by the interplay of the core and halo populations when either can be anisotropic, for example, $A_c > 1$ and $A_h > 1$. Sarfraz et al. (2016) have proposed recently an idealized approach for the solar wind electrons,

assuming both their core and halo components bi-Maxwellian and thus minimizing their contrast. The quasi-linear study of the EMEC instability has shown in this case a central role of the anisotropic electrons from the core. However, the free energy of suprathermal electrons in a bi-Kappa distributed halo may enhance the implication of this component as already suggested by a linear approach (Lazar et al., 2014; Lazar, Pierrard, et al., 2017). In the present paper we model the anisotropic electrons according to the observations in the solar wind, assuming them well described by a dual distribution which combines a bi-Maxwellian core and a bi-Kappa halo, and provide a specific quasi-linear analysis for the same instability.

The paper is organized as follows. The velocity distribution functions are introduced in section 2, with emphasis on the dual Maxwellian-Kappa model for the anisotropic electrons. In section 3 we build the quasi-linear approach of the EMEC instability and provide linear and quasi-linear solutions for three representative cases. The first two cases assume only one component anisotropic, either the halo (case 1: $A_c = 1$ and $A_h > 1$) or the core (case 2: $A_c > 1$ and $A_h = 1$), to extract their individual implication. In the third case both the core and halo populations are assumed anisotropic (case 3: $A_{c,h} > 1$), enabling us to study the instability under their cumulative action. Quasi-linear time evolutions of waves and particle dynamics are compared with the particle-in-cell (PIC) simulations, which are designed to overcome previous limitations and capture the effects of suprathermal tails of the distribution. Section 4 summarizes our findings.

2. Insights From Observations: Dual Velocity Distributions

The solar wind fluxes of electrons are measured and transformed into the frame of bulk flow, such that the resulting velocity distributions reveal very often only a dual structure combining a quasi-thermal core (subscript *c*) and a suprathermal halo (subscript *h*) (Lazar et al., 2015; Maksimovic et al., 2005)

$$f(v_\parallel, v_\perp) = \sum_{a=c,h} f_a(v_\parallel, v_\perp) = f_c(v_\parallel, v_\perp) + f_h(v_\parallel, v_\perp). \tag{1}$$

Examples of nonstreaming electron distributions measured by Ulysses are shown in Lazar et al. (2014), Figures 1 and 2. The core and halo populations remain the principal constituents even in the presence of an additional strahl (or beaming) component (Stverak et al., 2008), unless this is enhanced by the energetic events like coronal mass ejections (CMEs). In the absence of energetic events, the electron halo seems to enhance with heliocentric distance at the expense of the strahl, making the dual core-halo structure even more evident at large distances from the Sun (Maksimovic et al., 2005). Stverak et al. (2008) have shown that the electron core is well reproduced by a bi-Maxwellian

$$f_c(v_\parallel, v_\perp) = \frac{n_c}{\pi^{3/2}\alpha_{\parallel,c}\alpha_{\perp,c}^2} \exp\left(-\frac{v_\parallel^2}{\alpha_{\parallel,c}^2} - \frac{v_\perp^2}{\alpha_{\perp,c}^2}\right), \tag{2}$$

and the anisotropic halo can be described by a bi-Kappa

$$f_h(v_\parallel, v_\perp) = \frac{n_h}{\pi^{3/2}\alpha_{\parallel,h}\alpha_{\perp,h}^2} \frac{\Gamma[\kappa]}{\kappa^{1/2}\Gamma[\kappa - 1/2]} \left(1 + \frac{v_\parallel^2}{\kappa\alpha_{\parallel,h}^2} + \frac{v_\perp^2}{\kappa\alpha_{\perp,h}^2}\right)^{-\kappa-1}, \tag{3}$$

which are gyrotropic (isotropic in the plane perpendicular to the magnetic field) distribution functions modeling bi-axis temperature anisotropies $T_\perp \neq T_\parallel$ in polar coordinates $(v_\perp \cos\phi, v_\perp \sin\phi, v_\parallel) = (v_x, v_y, v_z)$. Here n_c and n_h are the number densities, and $\alpha_{\parallel,\perp,c}$ and $\alpha_{\parallel,\perp,h}$ are thermal velocities defined by the corresponding temperatures as moments of second order

$$\frac{2k_B T_{\parallel,c}}{m} \equiv 2\int \mathrm{d}\mathbf{v} v_\parallel^2 f_c(v_\parallel, v_\perp) = \alpha_{\parallel,c}^2, \tag{4}$$

$$\frac{2k_B T_{\perp,c}}{m} \equiv \int \mathrm{d}\mathbf{v} v_\perp^2 f_c(v_\parallel, v_\perp) = \alpha_{\perp,c}^2, \tag{5}$$

$$\frac{2k_B T_{\parallel,h}}{m} \equiv 2\int \mathrm{d}\mathbf{v} v_\parallel^2 f_h(v_\parallel, v_\perp) = \frac{\kappa\alpha_{\parallel,h}^2}{\kappa - 3/2}, \tag{6}$$

$$\frac{2k_B T_{\perp,h}}{m} \equiv \int \mathrm{d}\mathbf{v} v_\perp^2 f_h(v_\parallel, v_\perp) = \frac{\kappa\alpha_{\perp,h}^2}{\kappa - 3/2}. \tag{7}$$

In order to characterize the plasma parameters essential for the instability, here we invoke the observational data set provided by Stverak et al. (2008) from more than 100,000 events detected by three spacecraft missions, Helios 1, Cluster II, and Ulysses. These events are limited to the ecliptic plane and have already been invoked in a series of studies of the core and halo electrons (Pierrard et al., 2016; Stverak et al., 2008). As already motivated above, relevant for the present study are only the slow wind ($V_{SW} < 500$ km/s) data with a reduced influence of the strahls. Thus, in the ecliptic during slow winds, the electron halo is much more dilute than the electron core, with a low number density not exceeding 10% of the total density of electrons $n_0 = n_c + n_h$, that is, $n_h/n_0 < 10\%$. The power index κ lies in the interval $2.6 \lesssim \kappa \lesssim 9.4$, from which we choose two particular (mean) values, $\kappa = 2.8$ found relevant for the events with a low κ, and $\kappa = 8$, representative for more "thermalized" halos. In the stability analysis another key parameter is the (parallel) plasma beta parameter $\beta_{\parallel,a} = 8\pi n_a T_{\parallel,a}/B_0^2$. The observations have shown that both the core and halo electrons concentrate at the equipartition condition $\beta_c \simeq \beta_h \simeq 1$ (Lazar et al., 2015; Stverak et al., 2008), suggesting that kinetic energy densities of these two populations are comparable and none of them can be ignored. Here we consider for the core $\beta_{c,\parallel} = 0.9$, and for the halo $\beta_{h,\parallel} \simeq 1.0$. The suprathermal halo is less dense but hotter than the core ($n_h << n_c$, $T_h > T_c$), and a halo beta parameter slightly higher than the core ($\beta_{h,\parallel} \gtrsim \beta_{c,\parallel}$) is expected to boost the effect of the suprathermal electrons on the instability.

3. EMEC Instability: Quasi-linear Approach

3.1. Kinetic Dispersion-Stability Formalism

We investigate the instability of the electromagnetic electron-cylcotron (EMEC) modes driven by anisotropic electrons with a temperature anisotropy $T_\perp > T_\parallel$. When the anisotropic electrons are described by a monotonous distribution function, like the one introduced in equation (1) with the components defined in equations (2) and (3), the fastest growing EMEC modes propagate parallel to the uniform magnetic field (Kennel & Petschek, 1966). In the linear approximation the general dispersion relation of the parallel EM modes reads (Lazar et al., 2014)

$$\frac{k^2c^2}{\omega^2} = 1 + \frac{4\pi^2}{\omega^2}\sum_a \frac{e_a}{m_a}\int_{-\infty}^{\infty}\frac{\mathrm{d}v_\parallel}{\omega - kv_\parallel \pm \Omega_a}\int_0^\infty \mathrm{d}v_\perp v_\perp^2\left[(\omega - kv_\parallel)\frac{\partial f_a}{\partial v_\perp} + kv_\perp\frac{\partial f_a}{\partial v_\parallel}\right], \tag{8}$$

where f_a is an arbitrary distribution function of particles of sort a, ω, and k are, respectively, the wave frequency and the wave number, c is the speed of light in vacuum, $\Omega_a = q_a B_0/(m_a c)$ is the (nonrelativistic) gyrofrequency, and "$\pm$" is used to distinguish between the circularly polarized modes with right-hand (RH) and left-hand circular polarizations, respectively. In parallel direction the EMEC modes are RH polarized and are decoupled from the electrostatic oscillations.

The contribution of ions (protons) to the high-frequency EMEC modes is minimal, and we can assume them Maxwellian, as in equation (2), and isotropic, that is, with $\alpha_{i,\perp} = \alpha_{i,\parallel} = \alpha_i$. Instead, the EMEC modes are driven by the interplay of the electron core ($a = c$) and halo ($a = h$) populations when either can be anisotropic with temperature anisotropies $A_{c,h} = (T_\perp/T_\parallel)_{c,h} > 1$. Thus, assuming these components described by equations (2)–(7), the dispersion relation (8) becomes

$$\frac{k^2c^2}{\omega^2} = \frac{\omega_{pi}^2}{\omega k\alpha_i}Z\left(\frac{\omega + \Omega_i}{k\alpha_i}\right) + \sum_{a=c,h}\frac{n_a}{n_0}\frac{\omega_{pe}^2}{\omega^2}\left[A_a - 1 + \frac{(A_a - 1)(\omega - |\Omega_a|) + \omega}{k\alpha_{a\parallel}}Z_a\left(\frac{\omega - |\Omega_a|}{k\alpha_{a\parallel}}\right)\right], \tag{9}$$

where $n_0 = n_i = n_e = n_c + n_h$, $\omega_{pe,i} = (4\pi n_0 e^2/m_{e,i})^{1/2}$ are the plasma frequencies for the electrons (subscript e) and ions (subscript i),

$$Z(\zeta) = \frac{1}{\pi^{1/2}}\int_{-\infty}^{+\infty}\mathrm{d}x\,\frac{\exp(-x^2)}{x - \zeta}, \tag{10}$$

is the Maxwellian plasma dispersion function (Fried & Conte, 1961) of argument $\zeta_i = (\omega + \Omega_i)/k\alpha_{\parallel,i}$, and for the electron core $Z_c(\zeta_c) = Z(\zeta_c)$ of argument $\zeta_c = (\omega - |\Omega_e|)/k\alpha_{\parallel,c}$, while for the halo component

$$Z_h(\zeta_h) = \frac{1}{\pi^{1/2}\kappa^{1/2}}\frac{\Gamma(\kappa)}{\Gamma\left(\kappa - \frac{1}{2}\right)}\int_{-\infty}^{\infty}\mathrm{d}x\,\frac{(1 + x^2/\kappa)^{-\kappa}}{x - \zeta_h}, \tag{11}$$

is the Kappa plasma dispersion function (Lazar et al., 2008) of argument $\zeta_h = (\omega - |\Omega_e|)/k\alpha_{\parallel,h}$.

In the diffusion approximation the general kinetic equation for the electron component of sort a reads (Sarfraz et al., 2016)

$$\frac{\partial f_a}{\partial t} = \frac{ie^2}{4m_e^2c^2}\frac{1}{v_\perp}\int_{-\infty}^{\infty}\frac{\mathrm{d}k}{k^2}\left[\left(\omega^* - kv_\parallel\right)\frac{\partial}{\partial v_\perp} + kv_\perp\frac{\partial}{\partial v_\parallel}\right] \times \frac{v_\perp \delta B^2(k,\omega)}{\omega - kv_\parallel + \Omega_a}\left[\left(\omega - kv_\parallel\right)\frac{\partial f_a}{\partial v_\perp} + kv_\perp\frac{\partial f_a}{\partial v_\parallel}\right], \tag{12}$$

where $a = c, h$, $\omega = \omega_k + i\gamma_k$ is the complex root of equation (9), and $\delta B^2(k)$ is the spectral wave energy density associated with electromagnetic cyclotron mode magnetic field perturbations, and described the wave kinetic equation

$$\frac{\partial \delta B^2(k)}{\partial t} = 2\gamma_k\,\delta B^2(k). \tag{13}$$

Initially described by equations (2)–(7), the core and halo components evolve in time under the effects of enhanced fluctuations. The second-order moments of their distributions are derived from equation (12)

$$\begin{aligned}\frac{\mathrm{d}T_{\perp a}}{\mathrm{d}t} &= -\frac{e^2}{2m_ec^2}\int_{-\infty}^{\infty}\frac{\mathrm{d}k}{k^2}\,\delta B^2(k)\left\{\left(\frac{2T_{\perp a}}{T_{\parallel a}} - 1\right)\gamma_k \right. \\ &\left. + \mathrm{Im}\,\frac{2i\gamma - |\Omega_e|}{k\alpha_{\parallel a}}\left[\frac{T_{\perp a}}{T_{\parallel a}}\,\omega - \left(\frac{T_{\perp a}}{T_{\parallel a}} - 1\right)|\Omega_e|\right] Z_a\left(\frac{\omega - |\Omega_e|}{k\alpha_{\parallel a}}\right)\right\}, \\ \frac{\mathrm{d}T_{\parallel a}}{\mathrm{d}t} &= \frac{e^2}{m_ec^2}\int_{-\infty}^{\infty}\frac{\mathrm{d}k}{k^2}\,\delta B^2(k)\left\{\frac{T_{\perp a}}{T_{\parallel a}}\,\gamma_k \right. \\ &\left. + \mathrm{Im}\,\frac{\omega - |\Omega_e|}{k\alpha_{\parallel a}}\left[\frac{T_{\perp a}}{T_{\parallel a}}\,\omega - \left(\frac{T_{\perp a}}{T_{\parallel a}} - 1\right)|\Omega_e|\right] Z_a\left(\frac{\omega - |\Omega_e|}{k\alpha_{\parallel a}}\right)\right\}.\end{aligned} \tag{14}$$

Growing fluctuations cannot be described independently of the evolving distributions (and their principal moments) because equations (13) and (14) are coupled and nonlinear. These equations can be solved only numerically and iteratively, and for a numerical analysis we introduce the following dimensionless quantities (Sarfraz et al., 2016): frequency, z (normalized to electron gyrofrequency), wave number, q (normalized to electron skin depth), halo electron density ratio, δ, proton-to-electron mass ratio, M, Z function arguments for ions (protons), ξ_i and ζ_i, as well as ion beta; core and halo electron Z_a function arguments, ζ_c and ζ_h, as well as quantities η_c and η_h; the anisotropy of the core and halo components, A_c and A_h, as well as their parallel betas, β_c and β_h; normalized time, τ (normalized to inverse electron gyroperiod), and normalized magnetic field wave energy density, $W(q)$ (normalized to ambient magnetic field energy density):

$$\begin{aligned} z &= \frac{\omega}{|\Omega_e|}, \qquad q = \frac{ck}{\omega_{pe}}, \qquad \delta = \frac{n_h}{n_0}, \qquad M = \frac{m_i}{m_e}, \\ \xi_i &= \frac{z}{q(M\beta_i)^{1/2}}, \quad \zeta_i = \frac{Mz+1}{q(M\beta_i)^{1/2}}, \quad \beta_i = \frac{8\pi n_0 T_i}{B_0^2}, \\ \zeta_c &= \frac{(1-\delta)^{1/2}(z-1)}{q\beta_{\parallel c}^{1/2}}, \quad \eta_c = \frac{(1-\delta)^{1/2}[A_c(z-1)+1]}{q\beta_{\parallel c}^{1/2}}, \\ \zeta_h &= \frac{(\delta\nu_\kappa)^{1/2}(z-1)}{q\beta_{\parallel h}^{1/2}}, \quad \eta_h = \frac{(\delta\nu_\kappa)^{1/2}[A_h(z-1)+1]}{q\beta_{\parallel h}^{1/2}}, \\ \nu_\kappa &= \frac{\kappa}{\kappa - 1.5}, \quad A_c = \frac{\beta_{\perp c}}{\beta_{\parallel c}}, \quad \beta_{\parallel,\perp c} = \frac{8\pi n_c T_{\parallel,\perp c}}{B_0^2}, \\ A_h &= \frac{\beta_{\perp h}}{\beta_{\parallel h}}, \quad \beta_{\parallel,\perp h} = \frac{8\pi n_h T_{\parallel,\perp h}}{B_0^2}, \\ \tau &= |\Omega_e|t, \qquad W(q) = \frac{\delta B^2(q)}{B_0^2}. \end{aligned} \tag{15}$$

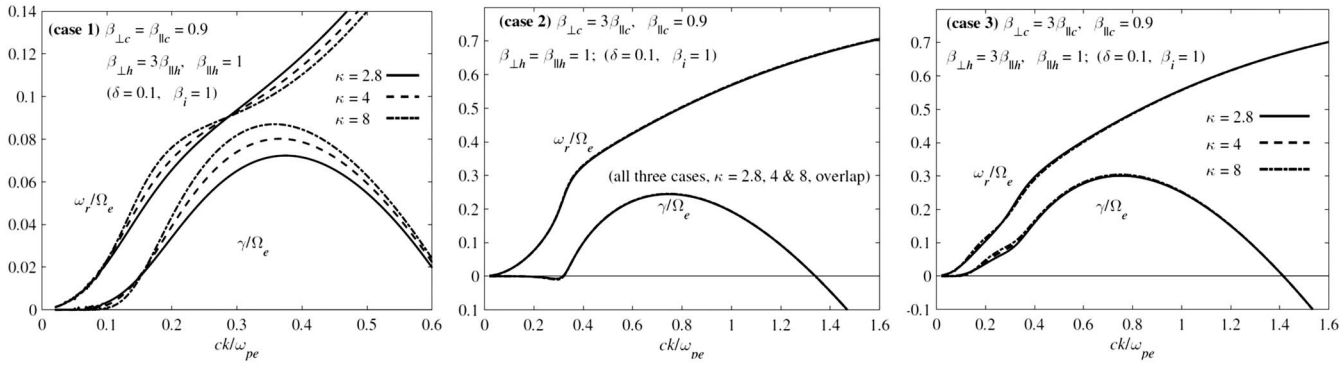

Figure 1. Linear EMEC (unstable) solutions: wave number dispersion of the wave frequency (ω_r) and the growth rate (γ) for three distinct cases, combining either an isotropic core and an anisotropic halo (case 1: $A_c = 1$, $A_h = 3$), or an anisotropic core with an isotropic halo (case 2: $A_c = 3$, $A_h = 1$), or when both the core and halo are anisotropic (case 3: $A_c = A_h = 3$).

The system of coupled of equations (9), (13), and (14) can be rewritten in terms of normalized quantites as

$$q^2 = \xi_i Z(\zeta_i) + (1-\delta)\left[A_c - 1 + \eta_c Z(\zeta_c)\right] + \delta\left[A_h - 1 + \eta_h Z_\kappa(\zeta_h)\right], \tag{16}$$

$$\frac{\partial W(q)}{\partial \tau} = 2 z_i W(q). \tag{17}$$

$$\begin{aligned}
\frac{\mathrm{d}\beta_{\perp c}}{d\tau} &= -2(1-\delta)\int_0^\infty \mathrm{d}q\, \frac{W(q)}{q^2}\left[\left(2A_c - 1\right) z_i + \mathrm{Im}\left(2iz_i - 1\right)\eta_c Z(\zeta_c)\right],\\
\frac{\mathrm{d}\beta_{\|c}}{\mathrm{d}\tau} &= 4(1-\delta)\int_0^\infty \mathrm{d}q\, \frac{W(q)}{q^2}\left[A_c z_i + \mathrm{Im}\,(z-1)\,\eta_c Z(\zeta_c)\right],\\
\frac{\mathrm{d}\beta_{\perp h}}{\mathrm{d}\tau} &= -2\delta\int_0^\infty \mathrm{d}q\, \frac{W(q)}{q^2}\left[\left(2A_h - 1\right) z_i + \mathrm{Im}\left(2iz_i - 1\right)\eta_h Z_\kappa(\zeta_h)\right],\\
\frac{d\beta_{\|h}}{d\tau} &= 4\delta\int_0^\infty \mathrm{d}q\, \frac{W(q)}{q^2}\left[A_h z_i + \mathrm{Im}\,(z-1)\,\eta_h Z_\kappa(\zeta_h)\right],
\end{aligned} \tag{18}$$

3.2. Linear EMEC Instability

We have studied the unstable EMEC solutions for realistic values of plasma parameters suggested by the observations in the solar wind (Lazar, Pierrard, et al., 2017; Pierrard et al., 2016; Stverak et al., 2008) and indicated in the previous section. Precisely, we assume the following initial ($t = 0$) parameters: $\delta(0) = (n_h/n_0)(0) = 0.1$, $(n_c/n_0)(0) = 1 - \delta(0) = 0.9$, $\beta_i(0) = 1 \simeq \beta_{\|,c}(0) = 0.9$, and $\beta_{\|,h}(0) = 1.0$. Primary information is given by the linear solutions of the dispersion relation (16), which can help us to distinguish between different regimes of the instability. Figure 1 displays the wave number ($q = ck/\omega_{pe}$) dispersion of normalized frequency ($z_r = \omega_k/\Omega_e$) and growth rate ($z_i = \gamma_k/\Omega_e > 0$) for three representative cases.

Case 1 assumes, for the initial conditions, the core isotropic $A_c(0) = 1$, and the halo anisotropic with $A_h(0) = 3$. Minimizing the core anisotropy may be found justified by the fact that core electrons are more thermalized than the halo electrons, and it should be definitely more realistic than other extreme scenarios which assume the core cold (see comments in Lazar et al., 2015, and Lazar, Pierrard, et al., 2017, and some references therein).

Case 2 considers the opposite situation with an anisotropic core with $A_c(0) = 3$ and an isotropic halo, $A_h(0) = 1$. Thinking that the core is (bi-)Maxwellian and more thermalized than the halo, this case may appear less realistic, but it should not be excluded from the analysis if we seek to understand the individual contributions of the core and halo populations.

Case 3 assumes both the core and halo anisotropic with the same anisotropy, that is, $A_c(0) = 3$ and $A_h(0) = 3$. This case is particularly important for decoding the interplay of these two populations. For all these cases the influence of suprathermal Kappa distributed electrons is studied by varying the power index with values indicated by the observations $\kappa = 2.8, 4, 8$ (see section 2). This influence becomes important leading to markedly distinct solutions only for a lower implication of the core component, for example, in case 1.

In case 1 the instability is driven by the anisotropic core and in case 2 by the anisotropic halo. Comparing cases 1 and 2 in Figure 1, we can observe that the unstable modes are driven by the anisotropic core at higher wave numbers and with higher growth rates than the halo instability. The presence of an isotropic halo has an inhibiting effect on the core instability (case 2) lowering the growth rates and leading even to damped modes ($\gamma < 0$) at lower wave numbers. Similar effects have been reported by the observations in the solar wind, where EMEC fluctuations appear to be damped by the suprathermal (halo) electrons (Wilson et al., 2013). In case 3 both components are assumed anisotropic and with same anisotropies. The halo peak shown by the growth rates is only hardly visible at low wave numbers, while the core peak is slightly enhanced by the cumulative effect of the anisotropic halo. The growth rates can be markedly enhanced by these cumulative effects for higher anisotropies of the core and halo components.

Deviations from isotropy may imply large values of plasma beta parameter, for example, $\beta_\perp > 2$. If reported by the observations, like those presented in Figures 5 and 6 (top panels) from Stverak et al. (2008), these values are associated with small anisotropies characteristic to quasi-stationary (stable) states. It is indeed less straightforward to capture the unstable plasma states, most probably due to the limitations of the measuring techniques. Observational data used to derive the anisotropy and the plasma beta parameter are measured and averaged over intervals of time relatively long (in general $\tau > 1$ min), making them relevant only for the quasi-stationary plasma states. For shorter time scales it is, however, reasonable to assume that higher anisotropies may exist but relax by inducing the instability investigated here. An extended quasi-linear approach can show the longer term effects of the instability, which may lead to the less anisotropic quasi-stationary states.

3.3. Quasi-Linear EMEC instability

In the quasi-linear (QL) analysis we follow the long-term evolution of the enhanced fluctuations, that is, the wave power $\delta B(t)^2/B_0^2$, and their back reaction on the velocity distributions of electrons enabling for changes of their temperatures and temperature anisotropy. We, however, keep a minimal number of constraints for the plasma system: the core and halo populations do not exchange particles, that is, $\delta = 0.1 =$ constant, and $\kappa =$ constant; the protons are not involved, that is, $\beta_i = 1 =$ constant, $A_p = 1 =$ constant. We assume the core and halo as two independent and closed plasma systems, ignoring any eventual effects of thermalization or suprathermalization but enabling the relaxation of the anisotropic particles as a result of their interaction with the enhanced fluctuations. In this case the plasma beta parameters can be considered as normalized temperatures, and the anisotropies of the electron populations can be defined implicitly by $A_c = \beta_{\perp,c}/\beta_{\parallel,c}$ and $A_h = \beta_{\perp,h}/\beta_{\parallel,h}$.

Figure 2 displays with red lines the numerical solutions of the QL equations (17) and (18), for all three cases introduced in the previous section: the evolution of plasma beta is shown in the left panels for the core ($\beta_{\perp,\parallel,c}$) and in the middle panels for the halo ($\beta_{\perp,\parallel,h}$), and the magnetic wave power $\delta B^2/B_0^2$ is plotted in the right panels. The influence of κ index becomes important only for cases 1 and 3, involving an anisotropic halo which relaxes faster when κ is higher. If κ is higher the instability grows faster, with higher growth rates, reducing the free energy and leading to enhanced fluctuations which are more efficient in the pitch angle isotropization and the relaxation process.

A transfer of free energy from the anisotropic to the isotropic components is obvious in cases 1 and 2, both components evolving with time in a sense that the anisotropic one is relaxed to lower anisotropies while the isotropic component becomes anisotropic. These two opposite evolutions become more evident in Figure 3, left and middle columns, which display temporal profiles of the anisotropies for both the core (bottom) and halo (top) components. However, the anisotropies reached in this case are much lower than the initial ones, that is, case 1: $A_h \simeq 1.06 < A_c \simeq 1.21 < A_h(0) = 3$, and case 2: $A_c \simeq 1.26 < A_h \simeq 1.36 < A_c(0) = 3$. To facilitate the analysis of the small anisotropies, we have zoomed into the temperature scale (y axis); see the first panel in case 1, and the second panel in case 2. Together, these evolutions may have a double significance. First, this is the second result that indicates a higher affinity of the halo component to absorb/damp the EMEC wave fluctuations. Second, these evolutions demonstrate that a small amount of free energy is exchanged by the electron components, and this transfer seems to be mediated by the instability itself. We can also evaluate the energy budget and see how the energy is partitioned between the fluctuations and the electron components. For instance, in case 1 from the kinetic energy lost by the halo (e.g., $\kappa = 2.8$: $\Delta\beta_h \simeq 0.38$) only 5–10 % is gained by the core ($\Delta\beta_c \simeq 0.02$), and this is comparable with the amplitude of the magnetic (normalized) wave power ($\delta B^2/B_0^2 \simeq 0.032$). At later stages after saturation the halo is completely relaxed, maintaining at a small and constant anisotropy, while both the core anisotropy and the wave power continue apparently to decrease.

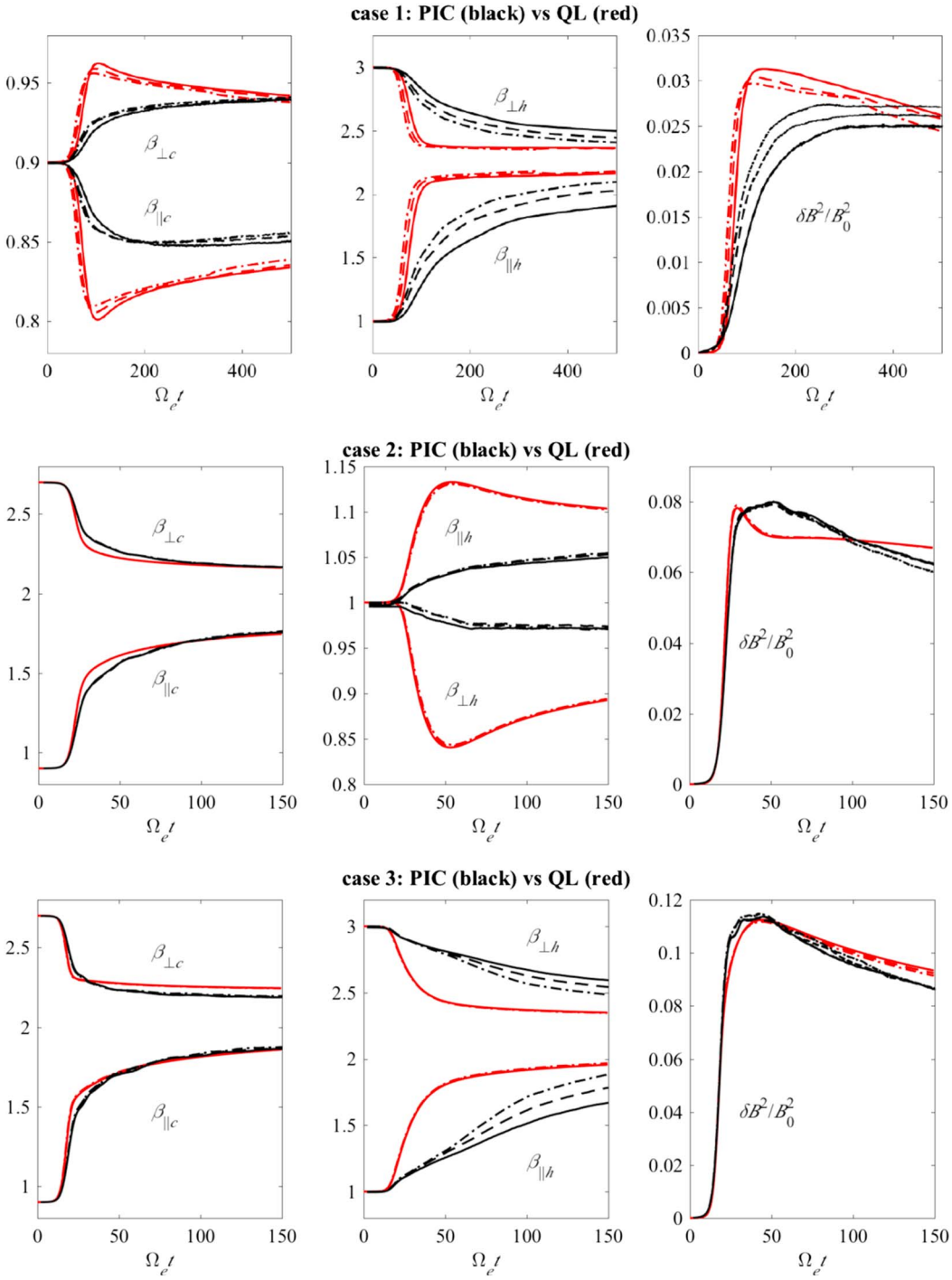

Figure 2. Time evolution from QL theory (red) and simulations (black): plasma betas for the core, (left column) $\beta_{\perp,c}$ and $\beta_{\parallel,c}$, and the halo, (middle column) $\beta_{\perp,h}$ and $\beta_{\parallel,h}$, and the wave energy density (right column) $\delta B^2/B_0^2$. Rows correspond to cases 1, 2, and 3, and plotting styles to the different κ values from Figure 1.

A similar analysis can be made in case 2 when the free energy is ceded/lost by the core and is partially gained by the halo. By comparison to case 1 the wave power transferred to the enhanced fluctuations is markedly increased (with a peak at $\delta B^2/B_0^2 \simeq 0.08$). Case 3 can be more realistic for the solar wind conditions as both the core and halo exhibit similar anisotropies, and the resulting instability leads to wave fluctuations of higher intensities ($\delta B^2/B_0^2 \simeq 0.108$) and to the relaxation of both these two components.

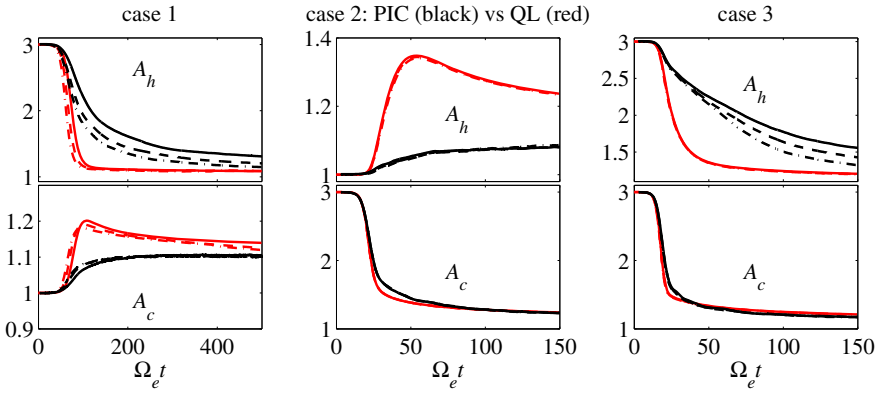

Figure 3. Time evolution of temperature anisotropy from QL theory (red) and PIC simulations (black) for the core (bottom row) and halo (top row) components for case 1 (left column), case 2 (middle column), and case 3 (right column).

3.4. PIC Simulations: Comparison With QL Theory

Here we present a comparative analysis with PIC simulations, with the intention to test the applicability of our QL approach. Let us first describe the setup and the parameters used in the simulations. We have built a 1.5D full particle-in-cell (PIC) code, where the spatial dimension is assumed in the $\hat{\mathbf{e}}_1$ direction and the constant background magnetic field is set to be $\mathbf{B}_0 = B_0\hat{\mathbf{e}}_1$. The simulation has periodic boundary conditions for both particles and fields. The plasma is assumed to be quasi collisionless, homogeneous, and composed of a single-proton species, described (initially) by isotropic Maxwellian distribution, and two electron particle species with realistic mass ratio $m_p/m_e = 1836$. The bi-Kappa electron component, that is, the distribution in equation (3), is generated by making use of the well-known accept-reject method. The box size is $L = 512c/\omega_{pe}$ (in terms of the electron inertial length), with $n_g = 4,096$ grid cells, and 1,500 particles per species per cell. The time step is $\Delta t = 0.01/\omega_{pe}$, and the ratio of electron plasma frequency and cyclotron frequency is $\omega_{pe}/|\Omega_e| = 10$. Notice that QL solutions do not depend explicitly on this frequency ratio, but to ensure a better energy conservation, values used in PIC simulations can be smaller (or much smaller) than observed in the solar wind.

The time evolutions obtained from simulations are shown in Figures 2 and 3 with black lines, for the same cases 1, 2, and 3 introduced above. We find a reasonable agreement between QL theory (red lines) and simulations (black lines), which confirm the relaxation of the temperature anisotropy and a transfer of free energy between the core and halo components. A good level of agreement is found for the evolution of Maxwellian core, which is less constrained by theoretical approach. The contrasting difference apparent in case 1 (Figure 2, left column) is only the result of the zoom (magnification) into the y axis scale. The same magnification is used in case 2 (Figure 2, middle column), to outline the anisotropization of the halo component. A rather large difference between QL approach and simulations is found for an initially anisotropic halo (cases 1 and 3). In these cases, the relaxation of the anisotropic components is more gradual in the simulations and the free energy transferred from anisotropic to isotropic components is less important than in QL approach. Later, after saturation, the asymptotic limit states may be highly dependent of the power index κ showing a better agreement with QL predictions, especially for a high power index, for example, $\kappa = 8$, (more thermalized halo). The time evolution of the magnetic wave power (right column) may also show some discrepancies, especially in case 1 when the instability is exclusively triggered by an anisotropic halo.

Figures 2 and 3 display and compare temporal profiles of the macroscopic properties describing the electrons and the enhanced fluctuations from QL theory and PIC simulations. Differences are not major and appear to be mainly associated with an initially anisotropic halo, suggesting certain limitations in the QL approach of this component, for example, $\kappa =$ constant, $\delta =$ constant. An evolution of these parameters can be indicated by the variations of the velocity distributions and their isolevels. Figure 4 shows in detail the time evolutions of the core and halo distributions, that is, f_c and f_h, respectively, for the same cases studied above, that is, case 1 (left), case 2 (middle), and case 3 (right). To represent these distributions, we plot isocontour levels 10^{-1}, 10^{-2}, 10^{-3}, and 10^{-4} of normalized distributions, $f_c/f_{c,\max}$ for the core and $f_h/f_{h,\max}$ for the halo. The QL results are displayed with red lines, and the simulations are reproduced in black. A qualitative analysis becomes straightforward in this case as the interval between isocontours should increase for a (bi-)Kappa with

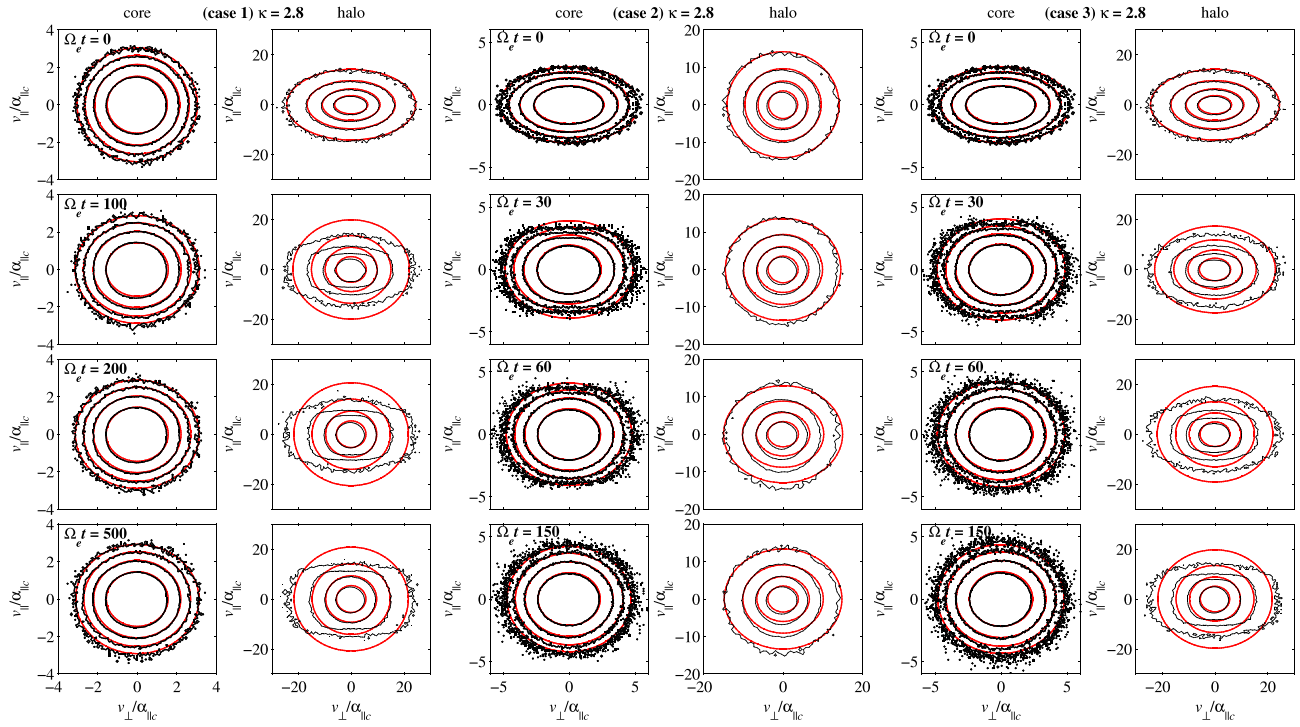

Figure 4. Time evolution of velocity distributions from QL theory (red) and PIC simulations (black) for $\kappa = 2.8$, $\delta = 0.1$, and $\omega_{pe}/|\Omega_e| = 10$, for case 1 (left column), case 2 (middle column), and case 3 (right column).

low values of power index $\kappa \to 2$ and should decrease for a (bi-)Maxwellian or a (bi-)Kappa with large values of power index $\kappa > 10$. Comparing the red and black contours, we can observe a number of distinct evolutions: (a) variations of their shapes due to a decrease or an increase of the temperature anisotropy, analyzed in Figure 2; (b) a slight increase of the interval between the halo contours, for example, in cases 1 and 3 with an initially anisotropic halo, that may prove a lowering of κ. Moreover, the relaxation of initially anisotropic halo occurs first at lower energies (higher isocontours, e.g., 10^{-1} and 10^{-2}), while the more energetic particles, which are, however, less representative, remain longer anisotropic; (c) minor changes indicating a uniform shrink of the core contours accompanied by a uniform expand of the halo contours, for example, cases 2 and 3, which suggest an exchange of particles between the core and halo components. The last two particular evolutions of the isocontours appear to be a result of particles suprathermalization (particles acceleration) by the enhanced fluctuations.

These results are also consistent with the instability evolutions from different plasma setups. Thus, Figures 5 and 6 display, respectively, the anisotropies and velocity distributions for $\delta = 0.05$ and $\omega_{pe}/|\Omega_e| = 15$ (PIC simulations with 1,000 particles per cell per species), showing similar contrasting evolutions as described above. Comparison of these results, for example, in Figures 3–6, confirms that eventual discrepancies between QL theory and simulations are associated in principal with the halo component (e.g., case 1 and case 3) and can be a direct consequence of the constraints imposed in theoretical modeling of this component (e.g., $\kappa =$ constant, $\delta =$ constant).

4. Summary and Conclusions

In the present paper we have carried out a quasi-linear (QL) analysis of the EMEC instability, for the first time in conditions revealed by the observations in the solar wind, where the electron velocity distributions exhibit a dual structure combining a bi-Maxwellian core and a bi-Kappa halo. Theoretical formalism for the dispersion and stability of this dual plasma system is provided in section 3.1, and it is used to describe linear instabilities (section 3.2) and quasi-linear effects of the enhanced fluctuations (section 3.3) for three representative cases assuming the core and halo components with different or similar anisotropies. A quasi-linear approach is particularly important as it enables a self-consistent description of the anisotropic particle dynamics and

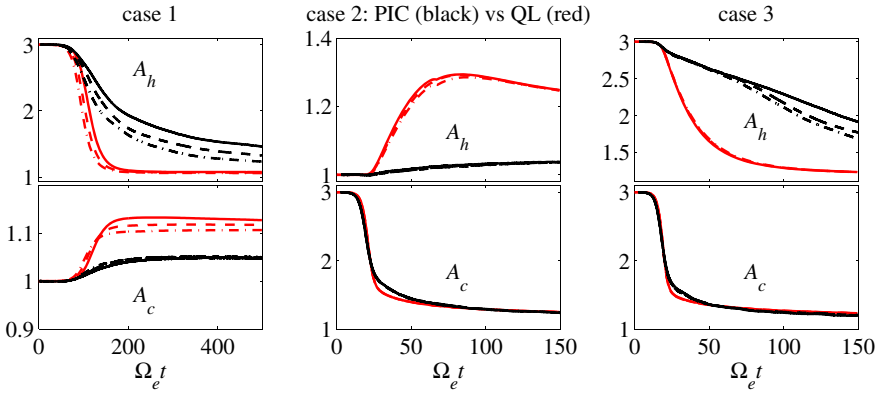

Figure 5. The same as in Figure 3 but for $\delta = 0.05$ and $\omega_{pe}/|\Omega_e| = 15$.

the resulting instabilities and may help in understanding the origin and implications of the wave fluctuations in space plasmas. The validity of our QL approach has been tested within PIC simulations and a comparative analysis is presented in section 3.4.

The interplay of the core and halo anisotropy becomes obvious from the linear stage of instability (Figure 1), when, for instance, the growth rates are markedly enhanced by the cumulative effect of these two components (case 3). The halo component plays a major role only when the core is less anisotropic (case 1), and in that case the wave frequency and growth rates become highly dependent of the power index κ. In the opposite case, a less anisotropic halo inhibits the instability driven by the core (case 2), a result that seems to agree with the observations which show that EMEC fluctuations detected in the solar wind are damped by the suprathermal (halo) electrons (Wilson et al., 2013). Both the core and halo populations continue to be involved in the QL approach of the instability (Figures 2–6), depending of their anisotropy. Figures 2, 3, and 5 present the long-term evolutions of the macroscopic plasma beta parameters and the magnetic wave power, while Figures 4 and 6 show details of the velocity distributions.

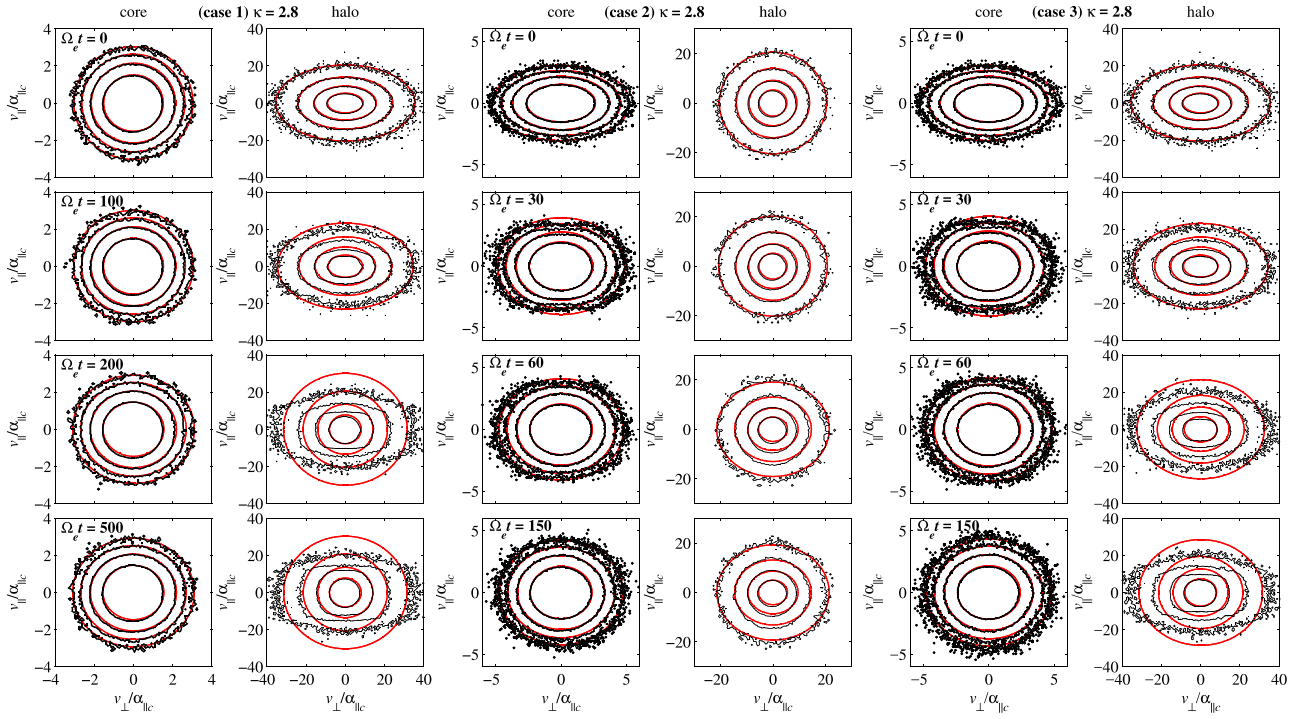

Figure 6. The same as in Figure 4 but for $\delta = 0.05$ and $\omega_{pe}/|\Omega_e| = 15$.

The effects of varying the value of κ agree with those obtained in previous studies with simplified models, assuming the electrons well described by a global bi-Kappa, which incorporates both the core and halo components (Eliasson & Lazar, 2015; Lazar et al., 2013; Lazar, Yoon, & Eliasson, 2017). Thus, if the temperature is assumed independent of κ and the (initial) anisotropy is large enough, the instability growth rates are enhanced with increasing κ, and the anisotropy relaxation becomes faster. These effects are most pronounced in the bi-Maxwellian limit ($\kappa \to \infty$), which is reproduced here by a bi-Kappa with $\kappa = 8$. Physically, the instability is stimulated by an excess of hot electrons, which are enhanced with increasing the κ values, see Figure 2 in Lazar (2017) for a comparison with Maxwellian limit. On the other hand, deviations of the bi-Kappa computations with lower values of κ, for example, $\kappa = 2.8$, are only marginal, suggesting that the instability is not very sensitive to the shape of halo distribution function and future studies may adopt a standard bi-Maxwellian model for the electron halo (Sarfraz et al., 2016). A higher contrast should be expected when the halo component is more dense, for example, at high latitudes far from the ecliptic where the relative density η exceeds 20ϛ*percnt*; (Maksimovic et al., 2005), and in that an accurate description using bi-Kappa distribution functions would still be needed. Moreover, in the complementary case assuming the halo temperature dependent on κ, the effects of varying κ are opposite and the instability appears to be markedly (and systematically) enhanced by the suprathermal electrons (Lazar, 2017). These expectations remain to be confirmed by the future investigations.

Temporal evolutions predicted by the theory show a reasonable agreement with the simulations. QL theory may not consider some of nonlinear features that are always present in PIC simulations, but if the slopes are similar we can state a qualitative agreement; see, for example, Moya et al. (2012). Figures 2, 3, and 5 compare the macroscopic plasma beta parameters and the magnetic wave power. The level of agreement depends on the power index κ and improves for higher values, for example, $\kappa = 8$ (thermalized halo), that means for a lower contrast between the core and halo components. It becomes also evident that the interplay of these two components is mediated by the instability and highly depends of the initial conditions. The highest wave power densities are reached when both components are initially anisotropic (case 3). In the relaxation process the QL theory predicts a quick relaxation of the anisotropy, which is confirmed by the PIC simulations but only for the core component. The halo anisotropy has instead a gradual lowering evolution, on a longer time scale. On the other hand, for cases 1 and 2 the long-term analysis may reveal a transfer of (free) energy from the anisotropic component to the less anisotropic one. The simulations confirm this transfer but at slightly lower magnitudes. Differences between QL theory and PIC simulations, although not major, appear to be triggered by the halo population (especially when this component is initially anisotropic—cases 1 and 3) suggesting certain limitations in theoretical approach of this component. Indeed, for the sake of simplicity we have assumed $\delta =$ constant and $\kappa =$ constant, and an eventual exchange of particles between core and halo during the relaxation process cannot be captured in the present QL theory. In order to check the validity of these assumptions, we have looked to the evolutions of the velocity distributions and their isolevels (10^{-1}, 10^{-2}, 10^{-3}, and 10^{-4}) within PIC simulations, for example, in Figures 4 and 6, and their variations confirm that these parameters may suffer alterations during the anisotropy relaxation. By contrast to the core, the relaxation of an initially anisotropic halo occurs also gradually beginning with the lower energy populations. The present results suggest that for Kappa distributed populations, a standard QL approach accounting only for the evolution of the main moments of the velocity distribution may not offer a detailed description for the instability saturation and the anisotropy relaxation. The approach seems to be altered by the parameters constrained to remain constant, for example, δ and κ quantifying the suprathermal (halo) population. Moreover, when dealing with complex distributions combining two contrasting components like a (bi-)Maxwellian core and a (bi-)Kappa halo, the energy constants, which must be exact consequences of the nonlinear equations for arbitrary-amplitude electron whistler disturbances (Davidson & Hammer, 1972), may need reformulation in order to account for the interplay of these components. Future investigations should seek for more insights from PIC or/and Vlasov simulations, which can suggest how to recalibrate in this case the QL approach and quantify the evolution of some key parameters like the power index κ and the density contrast δ which are constrained to remain constant in the present theory.

Despite the progress achieved in PIC simulations, which are now able to capture the effects of suprathermal tails on the kinetic instabilities in Kappa distributed plasmas, the numerical setups are still constrained to satisfy some restrictive conditions, for instance, the mean energy or/and the anisotropy of particles must be high enough to trigger the instability. Close to the energy equipartition $\beta_e \simeq 1$, the high energy required

for particles in simulations implies a frequency ratio $\omega_{pe}/|\Omega_e| \simeq 10$ markedly lower than the observations. Overcoming these limitations should be achievable in the future investigations and will enable realistic predictions and valuable confirmations for the QL approach of kinetic instabilities.

Acknowledgments
The present paper does not involve any spacecraft data analysis. However, upon request, numerical data for generating all the figures will be made available. M. L. acknowledge support in the framework of the projects GOA2316N (FWO-Vlaanderen) and SCHL 201/35-1 (DFG—German Research Foundation). P. H. Y. acknowledges NSF grant AGS1550566 to the University of Maryland, the BK21 plus program from the National Research Foundation (NRF), Korea, to Kyung Hee University, and the Science Award Grant from the GFT, Inc., to the University of Maryland. He also acknowledges the support from the Ruhr University Research School PLUS, funded by Germany's Excellence Initiative (DFG GSC 98/3), and by a Mercator fellowship awarded by the Deutsche Forschungsgemeinschaft through the grant Schl 201/31-1. R. A. L. acknowledges CONICyT for a Becas-Chile Postdoctoral fellowship 74160076 and CONICyT PIA project ACT1405. P. S .M. thanks CONICyT through FONDECyT grant 11150055 and CONICyT PIA project ACT1405.

References

Alexandrova, O., Chen, C. H. K., Sorriso-Valvo, L., Horbury, T. S., & Bale, S. D. (2013). Solar wind turbulence and the role of ion instabilities. *Space Science Reviews*, *178*, 101–139. https://doi.org/10.1007/s11214-013-0004-8

Bale, S. D., Kasper, J. C., Howes, G. G., Quataert, E., Salem, C., & Sundkvist, D. (2009). Magnetic fluctuation power near proton temperature anisotropy instability thresholds in the solar wind. *Physical Review Letters*, *103*, 211101.

Christon, S. P., Mitchell, D. G., Williams, D. J., Frank, L. A., Huang, C. Y., & Eastman, T. E. (1988). Energy spectra of plasma sheet ions and electrons from ∼50 eV/e to ∼1 MeV during plasma temperature transitions. *Journal of Geophysical Research*, *93*, 2562–2572.

Christon, S. P., Williams, D. J., Mitchell, D. G., Huang, C. Y., & Frank, L. A. (1991). Spectral characteristics of plasma sheet ion and electron populations during disturbed geomagnetic conditions. *Journal of Geophysical Research*, *96*, 1–22.

Collier, M. R., Hamilton, D. C., Gloeckler, G., Bochsler, P., & Sheldon, R. B. (1996). Neon-20, Oxigen-16, and Helium-4 densities, temperatures, and suprathermal tails in the solar wind determined with WIND/MASS. *Geophysical Research Letters*, *23*, 1191–1194.

Cuperman, S. (1981). Electromagnetic kinetic instabilities in multicomponent space plasmas: Theoretical predictions and computer simulation experiments. *Reviews of Geophysics and Space Physics*, *19*, 307–343.

Davidson, R. C., & Hammer, D. A. (1972). Nonequilibrium energy constants associated with large-amplitude electron whistlers. *Physics of Fluids*, *15*, 1282–1284. https://doi.org/10.1063/1.1694078

Eliasson, B., & Lazar, M. (2015). Nonlinear evolution of the electromagnetic electron-cyclotron instability in bi-Kappa distributed plasma. *Physics of Plasmas*, *22*, 062109.

Feldman, W. C., Asbridge, J. R., Bame, S. J., Montgomery, M. D., & Gary, S. P. (1975). Solar wind electrons. *Journal of Geophysical Research*, *80*, 4181–4196.

Fried, B. D., & Conte, S. D. (1961). *The plasma dispersion function*. New York: Academic Press.

Gaelzer, R., Ziebell, L. F., Vinas, A. F., Yoon, P. H., & Ryu, C.-M. (2008). Asymmetric solar wind electron superthermal distributions. *Astrophysics Journal*, *677*, 676–682.

Gary, S. P., & Feldman, W. C. (1978). A second-order theory for $k \parallel B_0$ electromagnetic instabilities. *Physics of Fluids*, *21*, 72–80. https://doi.org/10.1063/1.862081

Gary, S. P., Feldman, W. C., Forslund, D. W., & Montgomery, M. D. (1975). Heat flux instabilities in the solar wind. *Journal of Geophysical Research*, *80*, 4197–4203.

Gary, S. P., Jian, L. K., Broiles, T. W., Stevens, M. L., Podesta, J. J., & Kasper, J. C. (2016). Ion-driven instabilities in the solar wind: Wind observations of 19 March 2005. *Journal of Geophysical Research: Space Physics*, *121*, 30–41. https://doi.org/10.1002/2015JA021935

Gary, S. P., Moldwin, M. B., Thomsen, M. F., Winske, D., & McComas, D. J. (1994). Hot proton anisotropies and cool proton temperatures in the outer magnetosphere. *Journal of Geophysical Research*, *99*, 23,603–23,6015.

Hamasaki, S., & Krall, N. A. (1973). Relaxation of anisotropic collisionless plasma. *Physics of Fluids*, *16*, 145. https://doi.org/10.1063/1.1694161

He, J., Wang, L., Tu, C., Marsch, E., & Zong, Q. (2015). Evidence of Landau and cyclotron resonance between protons and kinetic waves in solar wind turbulence. *The Astrophysical Journal Letters*, *800*, L31. https://doi.org/10.1088/2041-8205/800/2/L31

Hellberg, M., Mace, R., & Cattaert, T. (2005). Effects of superthermal particles on waves in magnetized space plasmas. *Space Science Reviews*, *121*, 127–139. https://doi.org/10.1007/s11214-006-5024-1

Hellinger, P., Trávníček, P., Kasper, J. C., & Lazarus, A. J. (2006). Solar wind proton temperature anisotropy: Linear theory and WIND/SWE observations. *Geophysical Research Letters*, *33*, L09101. https://doi.org/10.1029/2006GL025925

Howes, G. G. (2017). A prospectus on kinetic heliophysics. *Physics of Plasmas*, *24*, 055907. https://doi.org/10.1063/1.4983993

Karimabadi, H., Krauss-Varban, D., & Terasawa, T. (1992). Physics of pitch angle scattering and velocity diffusion, 1. Theory. *Journal of Geophysical Research*, *97*, 13,853–13,864. https://doi.org/10.1029/92JA00997

Kasper, J. C., Lazarus, A. J., Gary, S. P., & Szabo, A. (2003). Solar wind temperature anisotropies. *AIP Conference Proceedings*, *679*, 538–541. https://doi.org/10.1063/1.1618653

Kennel, C. F., & Petschek, H. E. (1966). Limit on stably trapped particle fluxes. *Journal of Geophysical Research*, *71*, 1. https://doi.org/10.1029/JZ071i001p00001

Lazar, M. (2017). Towards realistic characterization of the solar wind suprathermal populations and their effects. *Physics of Plasmas*, *24*, 034501. https://doi.org/10.1063/1.4977899

Lazar, M., Pierrard, V., Shaaban, S. M., Fichtner, H., & Poedts, S. (2017). Dual Maxwellian-Kappa modeling of the solar wind electrons: New clues on the temperature of Kappa populations. *Astronomy & Astrophysics*, *602*, A44. https://doi.org/10.1051/0004-6361/201630194

Lazar, M., Poedts, S., & Michno, M. J. (2013). Electromagnetic electron whistler-cyclotron instability in bi-Kappa distributed plasmas. *Astronomy & Astrophysics*, *554*, A64. https://doi.org/10.1051/0004-6361/201220550

Lazar, M., Poedts, S., & Schlickeiser, R. (2014). The interplay of Kappa and core populations in the solar wind: Electromagnetic electron cyclotron instability. *Journal of Geophysical Research: Space Physics*, *119*, 9395–9406. https://doi.org/10.1002/2014JA020668

Lazar, M., Poedts, S., Schlickeiser, R., & Dumitrache, C. (2015). Towards realistic parametrization of the kinetic anisotropy and the resulting instabilities in space plasmas. Electromagnetic electron-cyclotron instability in the solar wind. *Monthly Notices of the Royal Astronomical Society*, *446*, 3022–3033.

Lazar, M., Schlickeiser, R., & Poedts, S. (2012). Suprathermal particle populations in the solar wind and corona, in exploring the solar wind, ed. M. Lazar (InTech), Ch. 11. Retrieved from http://www.intechopen.com/books/exploring-the-solar-wind

Lazar, M., Schlickeiser, R., & Shukla, P. K. (2008). Cumulative effect of the Weibel-type instabilities in symmetric counterstreaming plasmas with kappa anisotropies. *Physics of Plasmas*, *15*, 042103.

Lazar, M., Yoon, P. H., & Eliasson, B. (2017). Electromagnetic cyclotron instabilities in bi-Kappa distributed plasmas: A quasilinear approach. *Physics of Plasmas*, *24*, 042110.

Lin, R. P. (1998). Wind observations of suprathermal electrons in interplanetary medium. *Space Science Reviews*, *86*, 61–78.

Lu, Q., Zhou, L., & Wang, S. (2010). Particle-in-cell simulations of whistler waves excited by an electron κ-distribution in space plasma. *Journal of Geophysical Research*, *115*, A02213. https://doi.org/10.1029/2009JA014580

Maksimovic, M., Gary, S. P., & Skoug, R. M. (2000). Solar wind electron suprathermal strength and temperature gradients: Ulysses observations. *Journal of Geophysical Research*, *105*(A8), 18,337–18,350.

Maksimovic, M., Pierrard, V., & Riley, P. (1997). Ulysses electron distributions fitted with Kappa functions. *Geophysical Research Letters*, *24*, 1151–1154.

Maksimovic, M., Zouganelis, I., Chaufray, J.-Y., Issautier, K., Scime, E. E., Littleton, J. E., … Elliott, H. (2005). Radial evolution of the electron distribution functions in the fast solar wind between 0.3 and 1.5 AU. *Journal of Geophysical Research*, *110*, A09104. https://doi.org/10.1029/2005JA011119

Marsch, E., Muehlhaeuser, K.-H., Schwenn, R., Rosenbauer, H., Pilipp, W. G., & Neubauer, F. M. (1982). Solar wind protons: Three-dimensional velocity distributions and derived plasma parameters measured between 0.3 and 1 AU. *Journal of Geophysical Research*, *87*, 52–72.

McComas, D. J., Bame, S. J., Feldman, W. C., Gosling, J. T., & Phillips, J. L. (1992). Solar wind halo electrons from 1–4 AU. *Geophysical Research Letters*, *19*, 1291–1294.

Moya, P. S., Viñas, A. F., Muñoz, V., & Valdivia, J. A. (2012). Computational and theoretical study of the wave-particle interaction of protons and waves. *Annales Geophysicae*, *30*, 1361–1369. https://doi.org/10.5194/angeo-30-1361-2012

Olbert, S. (1968). Summary of experimental results from M.I.T. detector on IMP-1. In R. D. L. Carovillano, J. F. McClay, & H. R. Radoski (Eds.), *Physics of the magnetosphere, astrophysics and space science library* (Vol. 10, pp. 641–659). Netherlands: Springer.

Pagel, C., Gary, S. P., de Koning, C. A., Skoug, R. M., & Steinberg, J. T. (2007). Scattering of suprathermal electrons in the solar wind: ACE observations. *Journal of Geophysical Research*, *112*, A04103. https://doi.org/10.1029/2006JA011967

Pavan, J., Vinas, A. F., Yoon, P. H., Ziebell, L. F., & Gaelzer, R. (2013). Solar wind strahl broadening by self-generated plasma waves. *The Astrophysical Journal Letters*, *769*, L30. https://doi.org/10.1088/2041-8205/769/2/L30

Pierrard, V., & Lazar, M. (2010). Kappa distributions: Theory and applications in space plasmas. *Solar Physics*, *267*, 153–174.

Pierrard, V., Lazar, M., Poedts, S., Stverak, S., Maksimovic, M., & Travnicek, P. M. (2016). The electron temperature and anisotropy in the solar wind. Comparison of the core and halo populations. *Solar Physics*, *291*, 2165–2179.

Pilipp, W. G., Miggenrieder, H., Montgomery, M. D., Muehlhaeuser, K.-H., Rosenbauer, H., & Schwenn, R. (1987). Unusual electron distribution functions in the solar wind derived from the Helios plasma experiment: Double-strahl distributions and distributions with an extremely anisotropic core. *Journal of Geophysical Research*, *92*, 1093–1101.

Pilipp, W. G., Muehlhaeuser, K.-H., Miggenrieder, H., Montgomery, M. D., & Rosenbauer, H. (1987). Characteristics of electron velocity distribution functions in the solar wind derived from the HELIOS plasma experiment. *Journal of Geophysical Research*, *92*, 1075–1092.

Sarfraz, M., Saeed, Sundas, Yoon, P. H., Abbas, G., & Shah, H. A. (2016). Macroscopic quasi-linear theory of electromagnetic electron cyclotron instability associated with core and halo solar wind electrons. *Journal of Geophysical Research: Space Physics*, *121*, 9356–9368. https://doi.org/10.1002/2016JA022854

Sagdeev, R. Z., & Shafranov, V. D. (1961). On the Instability of a plasma with an anisotropic distribution of velocities in a magnetic field. *Journal of Experimental and Theoretical Physics*, *12*, 130–132. https://doi.org/10.1002/2016JA022854

Seough, J., & Yoon, P. H. (2012). Quasilinear theory of anisotropy-beta relations for proton cyclotron and parallel firehose instabilities. *Journal of Geophysical Research*, *117*, A08101. https://doi.org/10.1029/2012JA017645

Seough, J., Yoon, P. H., Kim, K.-H., & Lee, D.-H. (2013). Solar-wind proton anisotropy versus beta relation. *Physical Review Letters*, *110*, 071103. https://doi.org/10.1103/PhysRevLett.110.071103

Shaaban, S. M., Lazar, M., Poedts, S., & Elhanbaly, A. (2017). The interplay of the solar wind proton core and halo populations: EMIC instability. *Journal of Geophysical Research: Space Physics*, *121*, 6031–6047. https://doi.org/10.1002/2016JA022587

Stverak, S., Travnicek, P., Maksimovic, M., Marsch, E., Fazakerley, A. N., & Scime, E. E. (2008). Electron temperature anisotropy constraints in the solar wind. *Journal of Geophysical Research*, *113*, A03103. https://doi.org/10.1029/2007JA012733

Vasyliunas, V. M. (1968). A survey of low-energy electrons in the evening sector of the magnetosphere with OGO 1 and OGO 3. *Journal of Geophysical Research*, *73*, 2839–2884.

Vocks, C., & Mann, G. (2003). Generation of suprathermal electrons by resonant wave-particle interaction in the solar corona and wind. *Astrophysics Journal*, *593*, 1134.

Vocks, C., Salem, C., Lin, R. P., & Mann, G. (2005). Electron halo and strahl formation in the solar wind by resonant interaction with whistler waves. *Astrophysics Journal*, *627*, 540.

Wilson, L. B., Koval, A., Szabo, A., Breneman, A., Cattell, C. A., Goetz, K., … Pulupa, M. (2013). Electromagnetic waves and electron anisotropies downstream of supercritical interplanetary shocks. *Journal of Geophysical Research: Space Physics*, *118*, 5–16. https://doi.org/10.1029/2012JA018167

Yoon, P. H., Kim, S., Choe, G. S., & Moon, Y.-J. (2016). Revised model of the steady-state solar wind halo electron velocity distribution function. *Astrophysics Journal*, *826*, 204.

Yoon, P. H., & Seough, J. (2012). Quasilinear theory of anisotropy-beta relation for combined mirror and proton cyclotron instabilities. *Journal of Geophysical Research*, *117*, A08102. https://doi.org/10.1029/2012JA017697

Yoon, P. H., Seough, J. J., Kim, K. H., & Lee, D. H. (2012). Empirical versus exact numerical quasilinear analysis of electromagnetic instabilities driven by temperature anisotropy. *Journal of Plasma Physics*, *78*, 47–54. https://doi.org/10.1017/S0022377811000407

Zimbardo, G., Greco, A., Sorriso-Valvo, L., Perri, S., Vörös, Z., Aburjania, G., … Alexandrova, O. (2010). Magnetic turbulence in the geospace environment. *Space Science Reviews*, *156*, 89–134. https://doi.org/10.1007/s11214-010-9692-5